Scanning Tunneling Spectroscopy of Lead-Substituted Bismuth Strontium Copper Oxide

by

Michelle Zimmermann

Submitted to the Department of Physics
in partial fulfillment of the requirements for the degree of

Bachelor of Science in Physics

at the

MASSACHUSETTS INSTITUTE OF TECHNOLOGY

June 2007

Author .....
Department of Physics
May 25, 2007

Certified by .....
Eric W. Hudson
Assistant Professor, Department of Physics
Thesis Supervisor

Accepted by .....
Professor David E. Pritchard
Senior Thesis Coordinator, Department of Physics

Scanning Tunneling Spectroscopy of Lead-Substituted Bismuth Strontium Copper Oxide

by

Michelle Zimmermann

Submitted to the Department of Physics
on May 25, 2007, in partial fulfillment of the
requirements for the degree of
Bachelor of Science in Physics

Abstract

The hole-doped cuprate $Bi_{2-x}Pb_xSr_2Cu_1O_{6+\delta}$ is doped with lead to the solubility limit of $x = 0.38$ and studied using STM/STS in the overdoped regime where $T_c < 2$K. Despite the high lead content, residual supermodulations are observed in the BiO plane. In agreement with previous studies on (Pb,Bi)-2201, there is no separation of the sample into Pb-rich and Pb-poor domains, nor is there a spectral correlation with Pb location. Differential tunneling conductance is modeled using the van Hove scenario, wherein modulated regions are shown to have higher values of E_{VHS} than flat regions. The consistency of parameters matching theoretical predictions to tunneling spectra suggest that E_{VHS} describes a significant part of the density of states.

Thesis Supervisor: Eric W. Hudson
Title: Assistant Professor, Department of Physics

Acknowledgments

I would first like to thank Eric Hudson, not only for his guidance on this project, but also for the opportunity to work with him this year. After exploring several different areas of physics I am glad I found my way to the interesting research in his group, which has encouraged me to continue my education in condensed matter physics.

I am also grateful to the the Hudson group as a whole for welcoming me and teaching me so much. I particularly thank Doug Wise, from whom I had already learned a good deal about what "real physics" is like as his student in Junior Lab.

Finally, many thanks to Adam Groce for his countless hours of moral support, and most of all to my mother Jill and sister Laura who have always believed in me even when I didn't.

Contents

List of Figures

Chapter 1

Introduction

Since the discovery of superconductivity nearly a century ago, scientists have been exploring many different factors that influence the properties of these materials, revealing a system that is perhaps more complex than it was originally imagined to be. While much research has been directed towards finding the highest possible critical temperatures T_c below which superconductivity occurs, there are many other important parameters which can help reveal exactly what conditions are necessary to observe superconductivity itself.

The family of compounds $Bi_2Sr_2Ca_nCu_{n+1}O_{2n+6+\delta}$ (BSCCO) contains several high-temperature superconductors. In this thesis I will examine the properties of the $n = 0$ case, $Bi_2Sr_2CuO_{6+\delta}$ (Bi-2201), which is characterized by its single copper-oxide plane. The presence of extra oxygen in the BiO layers dopes the sample with holes, and this hole-doping amount δ is the parameter against which the phase diagram is drawn. The phase diagram shows a parabolic "superconducting dome" region, the maximum of which reflects the optimal doping for the maximization of T_c. One can continue to increase the oxygen content, however, and move the sample out of the superconducting region. By studying the changes that occur through this transition, one can better isolate the conditions necessary for superconductivity to exist.

This thesis will focus on the overdoped regime in Bi-2201, where $T_c < 2$ K. Along with the additional oxygen, our sample was also doped with lead atoms (Pb^{2+}) in place of some of the bismuth, which is known to remove the supermodulation otherwise

present in the Bi-O planes but apparently has no spectroscopic effects. We examine our sample in a range of 5 to 15 K, low temperatures still above T_c. In the second chapter, I will further explain the known characteristics of Bi-2201 and its phase diagram.

The remainder of this thesis will concern our experimental procedures and observations. The scanning tunneling microscope used for this thesis was constructed by Professor Eric Hudson and his group in the MIT Department of Physics. The third chapter explains the technique of scanning tunneling microscopy (STM) and our experimental setup. The fourth chapter describes the topography we observe in (Pb,Bi)-2201 and the incomplete suppression of supermodulations. The fifth chapter describes the spectroscopy measurements we made and their modeling using the van Hove scenario. Finally, the sixth chapter will summarize our results and discuss implications for future research.

Chapter 2

Properties of (Pb,Bi)-2201

2.1 Superconductivity

Superconductivity was first discovered in 1911 by H. Kamerlingh Onnes [29], who observed the disappearance of resistance in mercury at liquid helium temperatures. In the years that followed, the same phenomenon was discovered in other materials, but it would take four decades for scientists to develop reliable theories to explain what they were seeing.

Several theoretical models have been proposed to describe superconductivity. The Ginzburg-Landau (GL) theory, proposed in 1950, is a phenomenological thermodynamic model of a complex order parameter ψ which describes how thoroughly a system is in its superconducting phase [10]. It also predicts two additional characteristic parameters, the coherence length ξ and the penetration depth λ. The Ginzburg-Landau parameter $\kappa = \lambda/\xi$ differentiates between Type I and Type II superconductors, for which the type number describes the order of the transition between normal and superconducting phases. In a Type I superconductor, $\kappa < 1/\sqrt{2}$, while in a Type II superconductor, $\kappa > 1/\sqrt{2}$.

The GL theory, while descriptive and useful, does not tell us anything about the mechanism behind superconductivity. In 1957 two theoretical advances were made which added meaningfully to this goal. BCS theory, named for Bardeen, Cooper, and Schrieffer who proposed it, describes superconductivity using quantum mechan-

ical principles [2]. According to the theory, electrons with opposite spin are pushed together by lattice deformations, and if the temperature is low enough form "Cooper pairs" which are not affected by lattice vibrations - that is to say, they travel through the material without experiencing resistance. A "low enough" temperature is defined by the critical temperature T_c. The binding energy of the Cooper pairs leads to a gap in the single-particle excitation energies, since a base level of energy must be supplied simply to split the pair apart.

Despite these developments, the discovery of high-temperature superconductors (HTSCs) by Bednorz and Müller in 1986 [3] was not accounted for by the existing theories. These were materials with T_c values significantly higher than the previously expected limit of 30 K, some reaching upwards of 130 K [15]. Scientists today have no cohesive theory that includes both high-temperature and normal superconductivity. Further study and characterization of HTSCs is necessary in order to develop a more complete understanding of this phenomenon.

2.2 The cuprates

Most currently known high-temperature superconductors are cuprates, materials containing copper oxide planes in which charge carriers travel. The bismuth strontium calcium copper oxide (BSCCO) family contains three HTSCs of the composition $Bi_2Sr_2Ca_nCu_{n+1}O_{2n+6+\delta}$ for $n = 0$, 1, and 2, respectively labeled Bi-2201, Bi-2212, and Bi-2223. These compounds share several characteristics which I will review before describing some particular aspects of Bi-2201, the subject of this thesis.

The cuprates are unlikely candidates for high-temperature superconductivity for several reasons. First, as ceramics they are typically insulators. It is not until they are doped with excess carriers that they become normal metals, or at low temperatures, superconductors [7]. Second, they are characterized by strong electron-electron correlation in the form of a large Coulomb repulsion. This would seem to make it unlikely that electrons could be pushed close enough together to form Cooper pairs, yet something does happen which leads to the same macroscopic result [6].

The electronic properties of cuprates are parameterized by the amount of excess carriers; in the case of BSCCO, the relevant quantity is the amount of oxygen in the BiO planes, since the O^{2-} atoms introduce additional holes. From the magnitude of the superconducting gap Δ_0 caused by the binding of Cooper pairs, we can find T_Δ, the critical temperature for the formation and separation of pairs. The phase stiffness ρ_s determines the temperature T_Σ at which the Cooper pairs become phase coherent. Both of these temperatures are believed to depend on carrier density as illustrated for the BSCCO family in Figure 2-1. The superconducting critical temperature T_c is $\min(T_\Delta, T_\Sigma)$ [9], an approximately parabolic shape which is known as the superconducting dome.

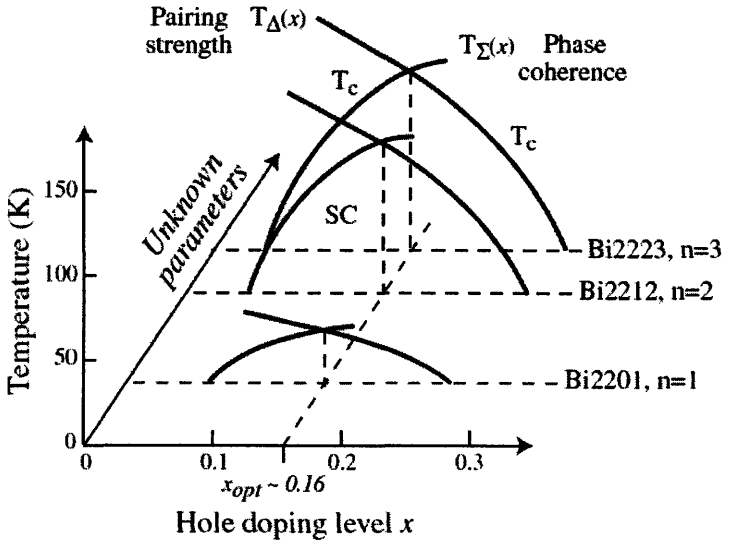

Figure 2-1: The phase diagram of BSCCO as a function of carrier density and number of CuO_2 planes [9].

2.3 (Pb,Bi)-2201

Bi-2201 is the $n = 0$ form of BSCCO. This means that its unit cell contains only a single CuO_2 layer. A diagram of the unit cell structure can be found in Figure 2-2. It has an orthorhombic structure, with lattice parameters given by $a = 5.362$ Å, $b = 5.374$Å, and $c = 24.622$ Å[16].

A sample of Bi-2201 with ideal composition would display a supermodulation throughout the crystal (Fig. 2-3). Topographical issues will be discussed in greater detail in Chapter 4. For introductory purposes it suffices to say that subsituting lead atoms for bismuth has been shown to remove the supermodulation [5, 12], making a sample easier to use for ARPES and other measurement techniques which would be adversely affected by such large-scale periodicity.

Single crystals of heavily Pb-substituted Bi-2201 can be grown using a floating zone method whereby two polycrystalline rods, each consisting of compressed powder of input compounds, are sintered and irradiated in air in an infrared furnace. As a molten zone formed by the irradiation is passed through one of the rods, the compound accumulates and an ingot is formed [5]. The extra carriers introduced by the lead substitution and the oxygen added by the in-air annealing will place a sample in the overdoped regime on the superconducting dome (marked in Fig. 2-4). Additionally, the crystal structure undergoes orthorhombic distortion, and the resulting lattice parameters are $a = 5.300$ Å, $b = 5.392$ Å, and $c = 24.603$ Å[5].

The samples used for this thesis were grown by Takeshi Kondo, now of Ames Laboratory, University of Iowa. The crystals were doped with lead to the solubility limit, where the lead content is approximately 19%. The samples of primary interest are also doped with oxygen such that $T_c < 2$K.

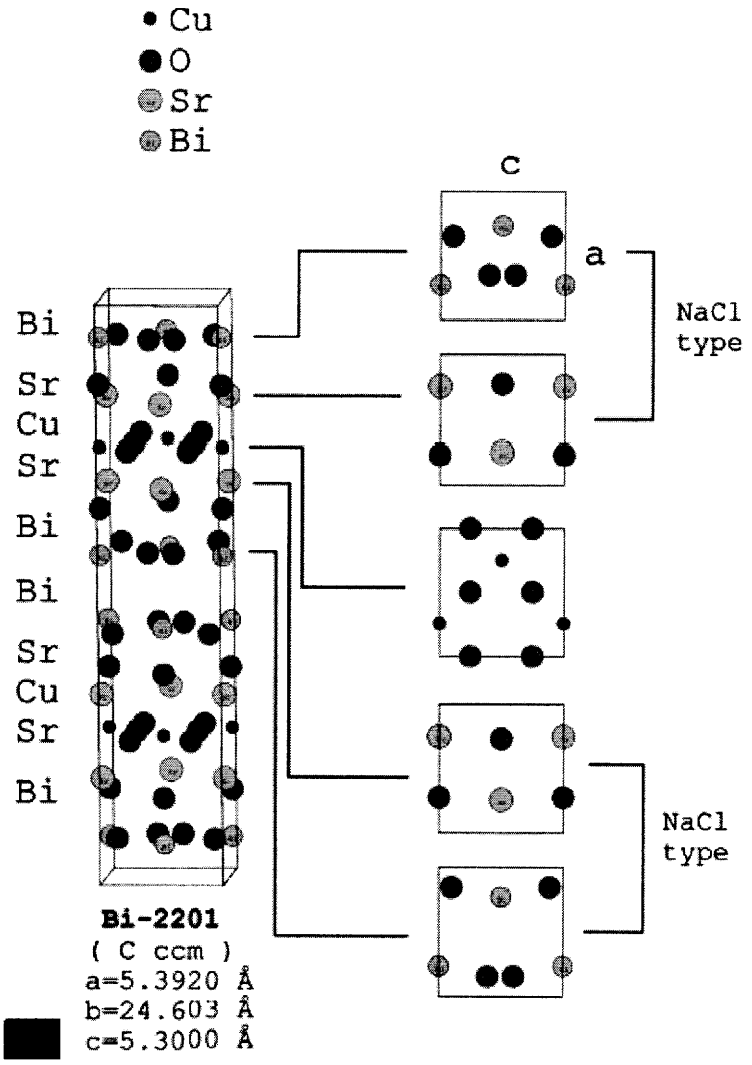

Figure 2-2: Two unit cells of Bi-2201 [16].

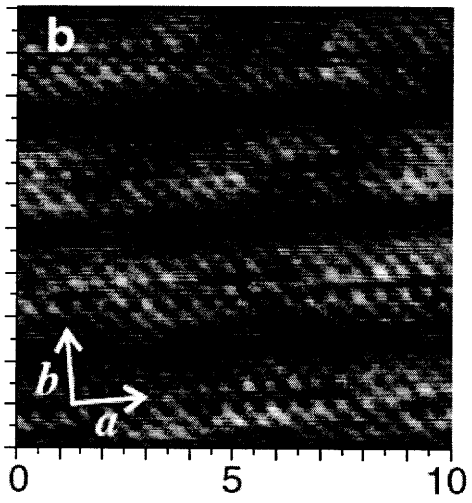

Figure 2-3: Supermodulation observed in Bi-2201 [19].

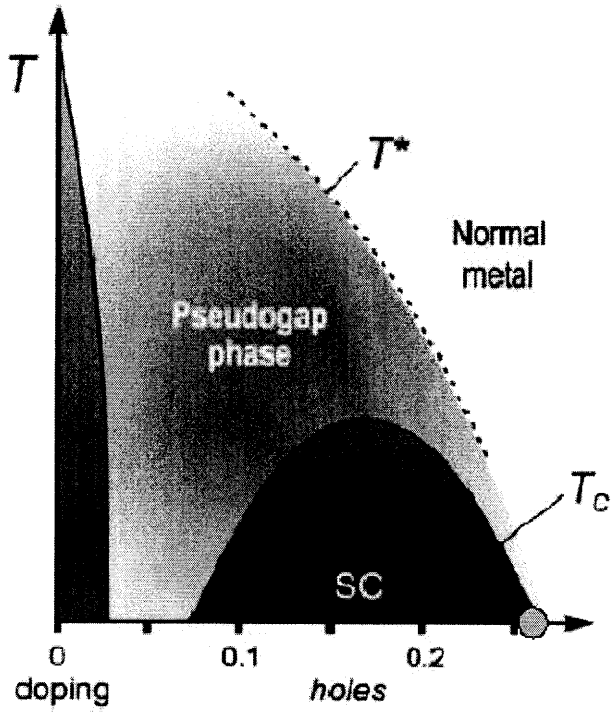

Figure 2-4: The phase diagram for Bi-2201. The region into which our sample falls is marked by a green circle.

Chapter 3

Experimental Procedures

The scanning tunneling microscope (STM) was invented in 1981 by Binnig and Rohrer [4], who received the 1986 Nobel Prize in Physics for their work. Scanning tunneling microscopy has become a popular technique in the last decades in part because of its high resolution and real-space presentation of measurements.

Professor Eric Hudson and his group at MIT use a home-built scanning tunneling microscope to examine the electronic properties of high-temperature superconductors. In this chapter I will describe the general principles and measurement techniques of scanning tunneling microscopy as well as the particular implementation details of the MIT STM.

3.1 Basics of STM

A scanning tunneling microscope (illustrated in Fig. 3-1) consists primarily of an atomically sharp probe tip which is brought to within 10 $\mathring{A}$ of a conductive or semiconductive material sample. When a small bias voltage is applied between the sample and the tip, electrons may tunnel through the thin but classically forbidden region of vacuum in order to move to a lower energy state.

STM measures the density of states available for an electron in the probe tip to move into. Following Mahan [22], we can calculate the tunneling probability of a

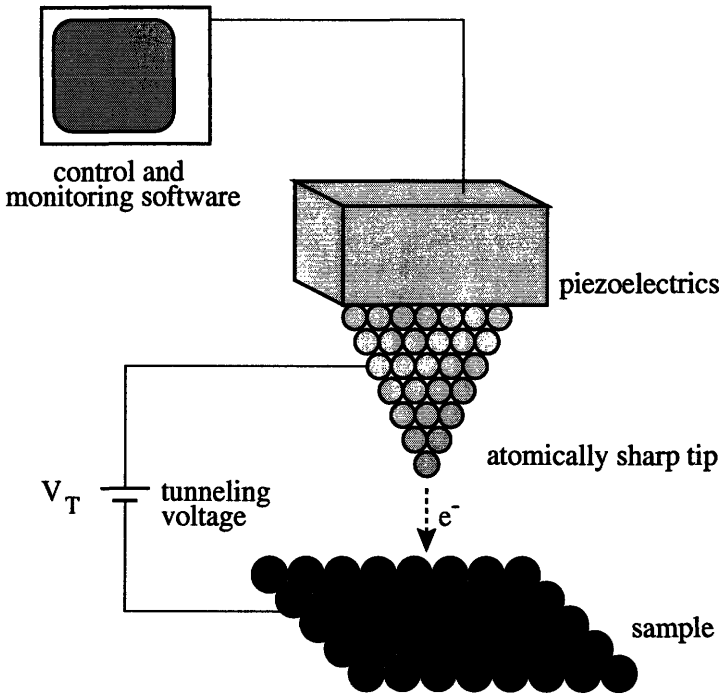

Figure 3-1: A schematic illustration of a scanning tunneling microscope.

single particle using the correlation function:

$$\chi(i\omega) = \sum_{k,p} |T_{k,p}|^2 \int_0^\beta d\tau \; e^{i\omega\tau} \mathcal{G}_R(k, -\tau)\mathcal{G}_L(p, \tau) \tag{3.1}$$

where p and the subscript L refer to the STM probe tip and k and the subscript R refer to the sample being probed (using the convention that electrons are tunneling from the tip to the sample, "left" to "right"). Broadening our view to the total tunneling current, we must consider the spectral functions A_L in the tip and A_R in the sample and integrate over all energies.

$$I = 2e \sum_{k,p} |T_{k,p}|^2 \int_{-\infty}^{\infty} \frac{d\epsilon}{2\pi} A_R(k, \epsilon) A_L(p, \epsilon + eV)[n_F(\epsilon) - n_F(\epsilon + eV)] \tag{3.2}$$

Summing over the k-space parameters and moving constant terms out of the integral, this can be rewritten as

$$I \propto \int_{-\infty}^{\infty} d\epsilon \; \rho_{tip}(\epsilon + eV)\rho_{sample}(\epsilon)[f(\epsilon + eV) - f(\epsilon)] \tag{3.3}$$

We can assume that ρ_{tip}, for a normal metal, is constant. Taking the derivative with respect to voltage we are simply extracting the sample density:

$$\frac{dI}{dV} \propto \rho_{sample} \tag{3.4}$$

Thus by measuring the changes in tunneling current with respect to voltage changes between the sample and the tip, one can extract a measure of the density of states in the sample.

There are several operating modes in which STM can be performed. By running the microscope in feedback mode, such that when the tip is moved over the sample the voltage automatically adjusts to maintain constant current, one can obtain a topographical image of the surface. The voltage will be turned lower when the tip is over regions which are elevated and turned higher when the tip is over regions which are depressed. By mapping the voltage to a color gradient we can interpret the data as a topographical image (see Fig. 3-2).

A second type of data can be recorded by leaving the tip in one location above the sample and measure the changes in tunneling current as the bias voltage is swept through a preset range. This provides a curve proportional to the local density of states in the sample (see Fig. 3-3). A final commonly useful data type is called a "spectral survey" and consists of a dI/dV curve taken at each point in a specified spatial grid. A spectral survey can be matched to a topography, allowing spectral

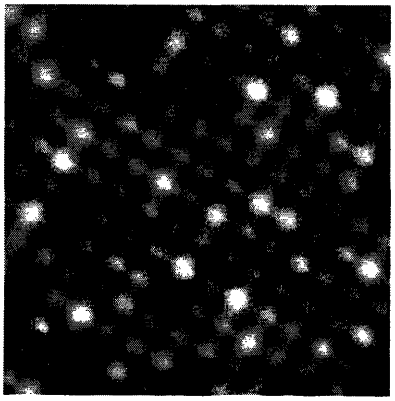

Figure 3-2: Example of a topography image from (Pb,Bi)-2201 (T_c=7 K). Pb atoms appear bright in the lattice of Bi atoms.

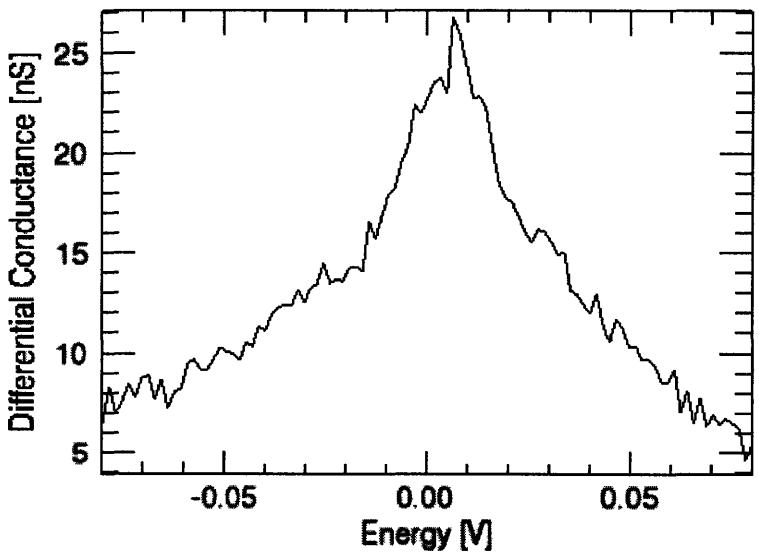

Figure 3-3: Example of a differential current spectrum from (Pb,Bi)-2201 (T_c <2K) measured at T =4.9K.

characteristics to be compared to visible features.

3.2 The MIT STM

The Hudson group at the Massachusetts Institute of Technology uses a home-built scanning tunneling microscope which has the capability to follow a particular atomically resolved region while changing the sample temperature. Figure 3-4 shows the precision imaging of one region at 5, 10, and then 15 K. Our STM is capable of temperatures in the range from 2 to 300 K, and functions at ultra-high vacuum ($< 10^{-8}$ Torr).

Figure 3-5 shows the main experimental apparatus, the STM and some key associated systems. There are several room-temperature systems which aid in stability and control. A set of counterweights on an adjustable-height platform is used to balance the Dewar weight and allow for raising and lowering by hand. An 8-foot sample control rod with a magnetic manipulation system moves the low-temperature stages. The outer frame, a granite slab between plates of (what?), is (describe floating mechanism) during experimental runs for vibration isolation.

The low-temperature systems, positioned inside the dewar, are designed for pre-

(a) T = 5 K. (b) T = 10 K. (c) T = 15 K.

Figure 3-4: The same atomically resolved region is found and imaged even as the temperature changes.

cision and convenience. Up to three different samples can be stored at once and switched into probing position while maintaining cryogenic temperatures and ultra-high vacuum. Below the sample storage stage is the cleaver, followed by an additional vibration isolation stage. The sample holder has four independent electrical contacts and holds the sample in place by means of a conical spring. The probe position sensor is a cylindrical capacitor that allows an approach over 5 mm by tuning the capacitance C from 7 to 12 pF. An Andeen-Hagerling bridge allows 10^{-19} F resolution, where a 100 Åstep translates to approximately 10^{-17} F.

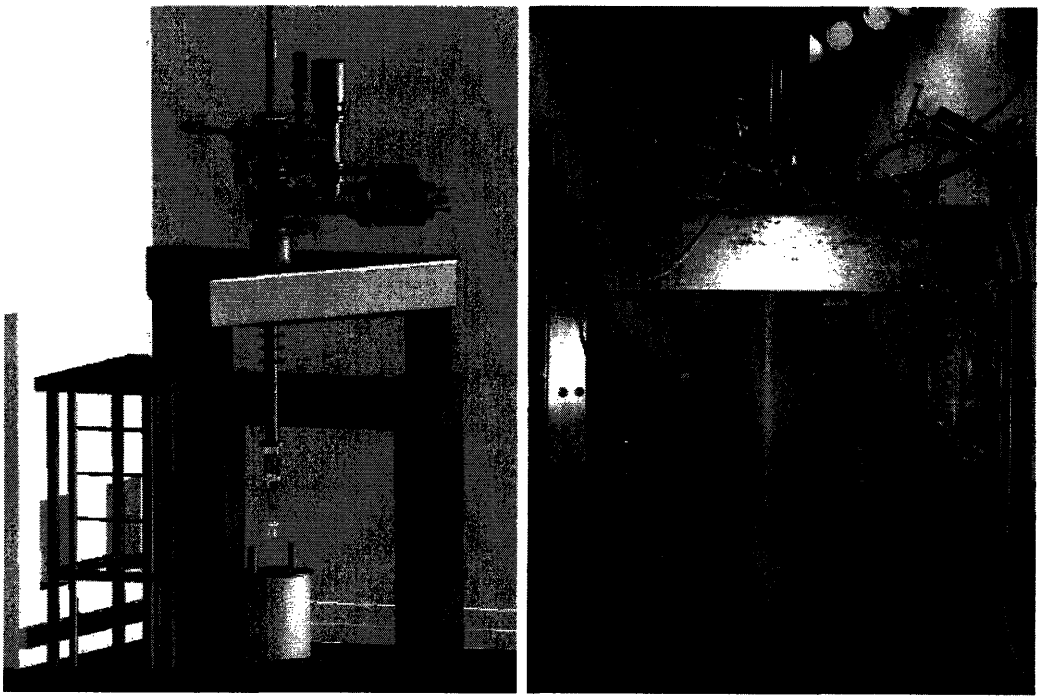

(a) (b)

Figure 3-5: The Hudson group's STM: (a) a schematic drawing; (b) a photograph.

Chapter 4

Topography of (Pb,Bi)-2201

One component of our studies on (Pb,Bi)-2201 is the characterization of observed topography. The weak binding between adjacent BiO layers faciliates the cleaving of the crystal betwen these planes, leaving an atomically smooth BiO layer for STM topographic imaging. Understanding the atomic structure we observe is useful for its own sake, particularly since the Bi atom spacing is the same as that of the copper atoms in the CuO_2 plane two layers below, but will also assist in a thorough analysis of spectral data. The atomic resolution of STM/STS has led to several discoveries of correlations between local topography and associated dI/dV spectra (see [1, 20, 26, 28] for some examples), so I will discuss the former here before delving further into the latter.

4.1 Supermodulation supression

A sample of $Bi_2Sr_2Cu_1O_{6+\delta}$ with ideal composition is consistently observed to have a regularly undulating rather than flat planar surface in its BiO layer. This is believed to be the result of excess oxygen in these layers, since modifications of BSCCO samples in ways that change their oxygen content also dependably change the modulation frequency [33, 17].

Substitution of lead (Pb^{2+}) atoms into a portion of BSCCO bismuth sites is understood to eliminate the supermodulation when enough substitutions are made [14].

Ikeda *et al.* [13] describe the preparation of a compound which has the chemical formula $Bi_{2-x+y}Pb_xSr_{2-y}Cu_{1+y/4}O_z$. They report the creation of two new modes that expand in wavelength as the Pb content is increased, finally canceling out all supermodulation at $x = 0.4$ and $y = 0.125$.

4.2 Lead content

Bright atoms in topography images are identified as lead atoms. The larger atomic radius of Pb^{2+} compared to Bi^{3+} means that the Pb sites are slightly closer to the tip and are mapped to a lower voltage by the STM in feedback mode. Analysis of topographical images by this identification yields a lead content of 18.9±1.6%. This quantity is in agreement with the atomic makeup of our sample, which was grown such that it contained 19% lead.

In contrast with studies on (Pb,Bi)-2212 [5, 18, 27] but in agreement with others on (Pb,Bi)-2201 [25], we did not observe organization of the sample into Pb-rich and Pb-poor regions. The lead atoms appear uniformly randomly distributed in the BiO planes.

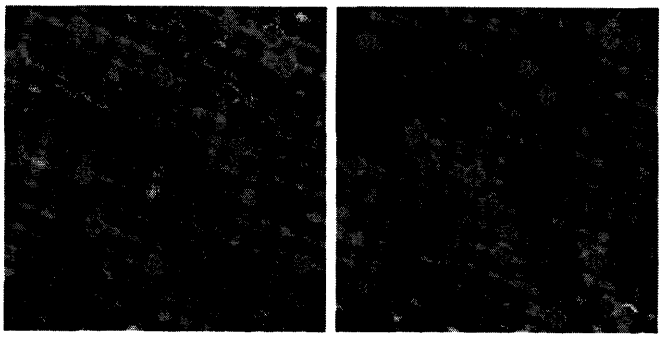

Figure 4-1: Lead atoms which have been substituted in the bismuth sites are marked with green circles.

4.3 Residual supermodulation

Despite the Pb-doping of our sample to near the solubility limit, we still observe a high degree of supermodulation remaining in our sample (Fig. 4-2). The modulations appear in small groups of between 2 and 5 "fingers", with each finger typically six atoms wide and ranging in length from approximately 200 to 500 Å.

Large-scale images such as the one in Figure 4-3 provide some added perspective to the issue. We observe mostly flat regions in between groups of fingers which consistently run parallel to each other. The modulated regions account for approximately 25% of the Bi0 plane. In flat regions, the lattice parameters a and b are nearly equal, measured to be 5.16±0.25 and 5.42±0.25 Å. In modulated regions, the lattice distorts in different ways depending on the direction of the local curvature: if the region is raised, $a = 5.23 \pm 0.22$ and $b = 6.11 \pm 0.29$ Å, while in depressed regions $a = 5.08 \pm 0.25$ and $b = 4.52 \pm 0.35$ Å.

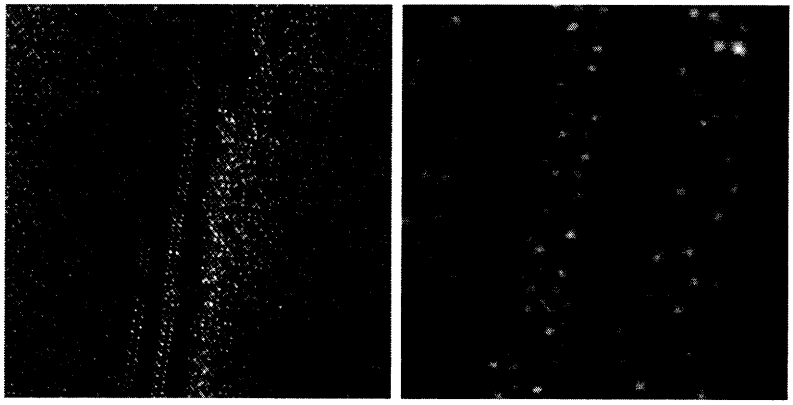

(a) (b)

Figure 4-2: Residual supermodulation in (a) a 100 Åimage and (b) a 350 Åimage.

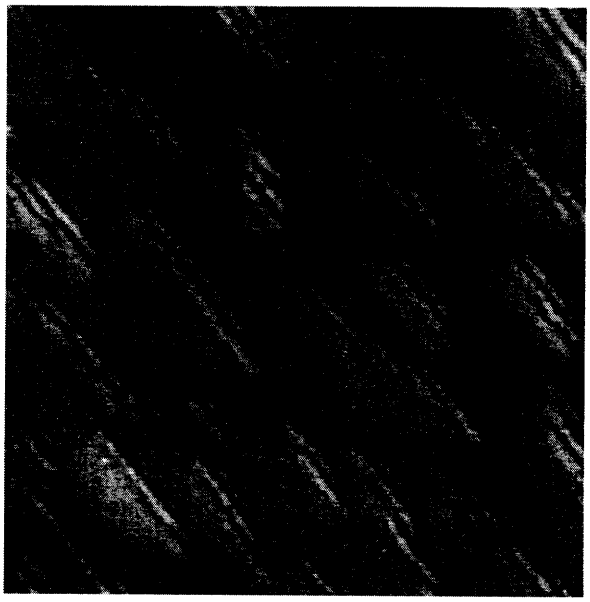

Figure 4-3: Residual supermodulation.

Chapter 5

Spectroscopy of (Pb,Bi)-2201

STM is useful for its high-resolution images of crystal surfaces, but STS (scanning tunneling spectroscopy) offers insight into materials' electronic properties. By measuring the dI/dV spectra with STS, we effectively see the density of states, which can help us to understand a variety of physical phenomena. For this reason, this chapter will detail the spectral characteristics we observe in overdoped (Pb,Bi)-2201 and argue in favor of a characterization by means of the van Hove scenario.

5.1 Spectroscopic data

The tunneling spectra we observed fall into three main types: peaks, split peaks, and gaps. Since the T_c of our sample is < 2K and all measurements are taken at $T > 4.5$K, the natural classification of the wide gaps is as pseudogaps rather than superconducting gaps [8, 21]. Below 15K we observe smaller gaps inside the broad gaps (Fig. 5-1), suggestive of the presence of local superconductivity above T_c. However, the gap features are very uncommon in our sample and are beyond the scope of this thesis. The dominant spectral types are the sharp conductance peak and the split peak, which can appear to be a gap on top of a peak but could also be interpreted as two peaks shifting between superimposed and separated (see Fig. 5-2).

We also examined spectral surveys in order to understand changes in the dI/dV curves as a function of position. Of particular interest were any changes which might

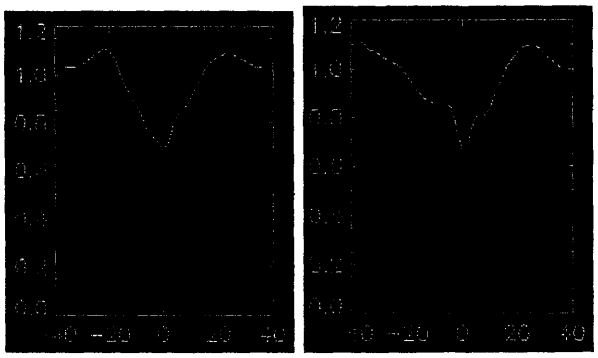

(a) (b)

Figure 5-1: (a) An example of the broad gap occasionally observed in (Pb,Bi)-2201. (b) A small gap appears within the broader gap. The x axis is measured in mV and the y axis is in arbitrary units representing conductance.

happen between modulated and flat regions of the BiO plane. Figure 5-3 shows two topographies on top of which spectral surveys were taken. The spectral data is then mapped according to three variables: peak width, peak height, and peak bias. (When multiple local maxima exist, the map reflects the one that represents the higher conductance.) The strongest connection is seen in the peak bias maps, where the spectra in the modulated regions are consistently at a lower energy than their counterparts in unmodulated areas. The peak width and height maps also suggest that on-modulation spectra are wider and shorter than the others. Spectral surveys also served to illustrate the lack of correlation between any particular spectral feature and the location of lead atoms.

5.2 Describing a tunneling spectrum

The general method for modeling differential tunneling conductance in STS relies on the differential current as a measure of the sample density of states. The tunneling-Hamiltonian formalism can be used to derive the expression [11]

$$\frac{dI}{dV} \propto -\int d\omega \sum_{\boldsymbol{k}} |T_k|^2 A(\boldsymbol{k}) f'(\omega - eV) \tag{5.1}$$

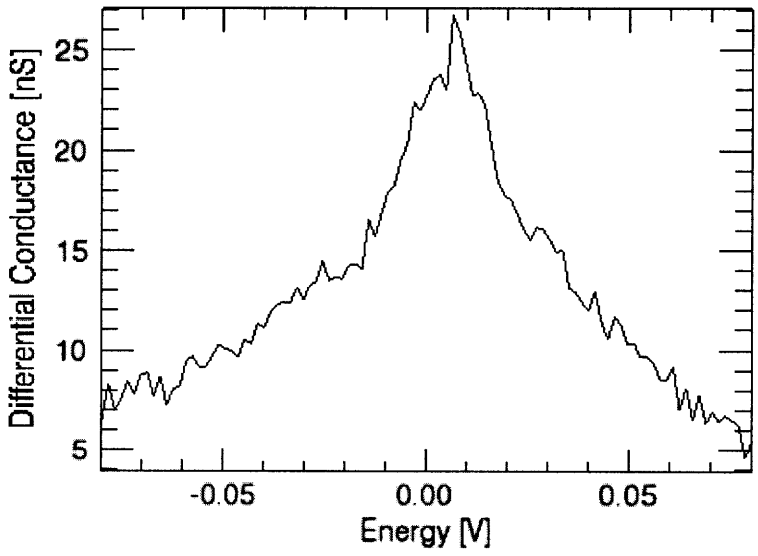

(a)

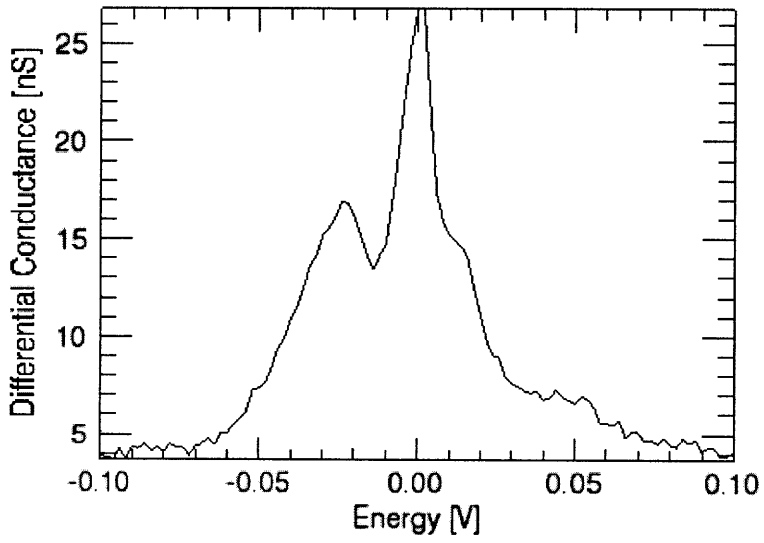

(b)

Figure 5-2: (a) An example of the conductance peak observed in (Pb,Bi)-2201. (b) The conductance peak splitting into two asymmetric peaks.

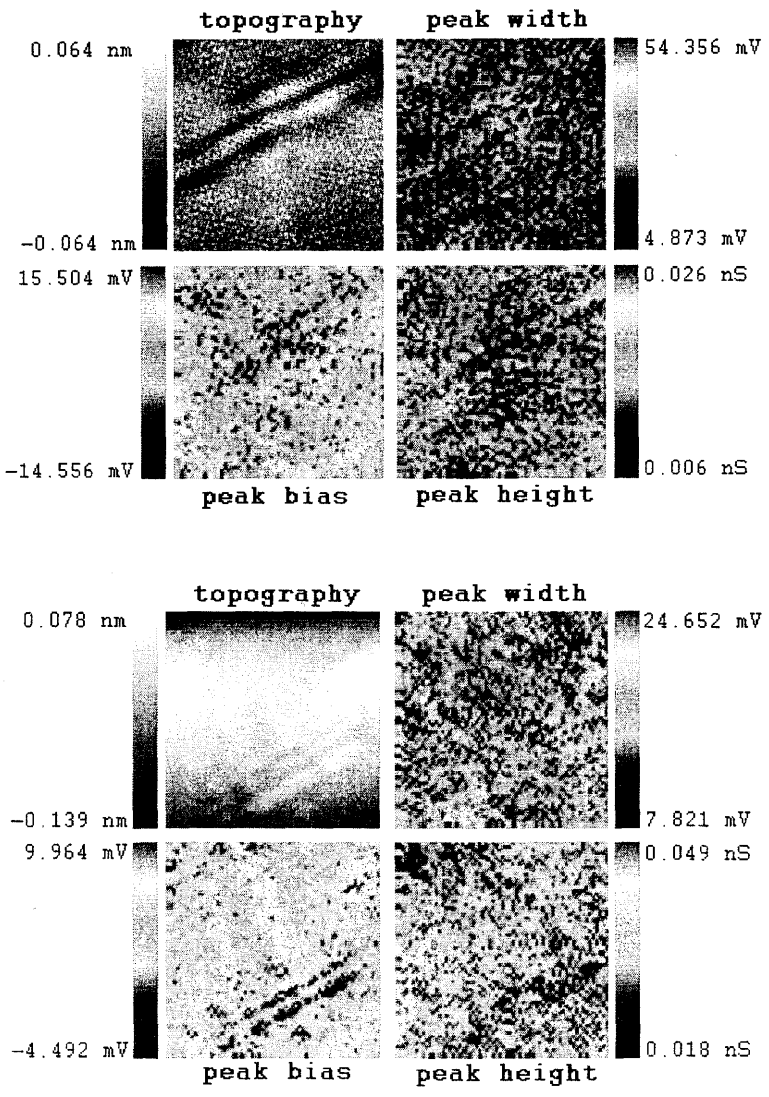

Figure 5-3: Spectral surveys allow the visualization of spectral relationships to topography.

Parameter	Value (eV)
t_0	0.435
t_1	-0.1
t_2	0.038
t_3	0.0
t_4	0.0

Table 5.1: Tight binding parameters.

where $A(\boldsymbol{k},\omega)$ is the spectral function and $f(E)$ is the Fermi function. Energies ω and eV are written by convention such that negative values are occupied states and positive values are unoccupied. The matrix element T_k is assumed to be energy-independent and isotropic, thus removable from the integrand. The spectral function is writtten

$$A(\boldsymbol{k},\omega) = -\frac{1}{\pi}\mathrm{Im}\left(\frac{1}{\omega - i\Gamma - \epsilon(\boldsymbol{k}) - \Sigma(\boldsymbol{k},\omega)}\right) \tag{5.2}$$

with Γ representing a lifetime broadening term set to 1 meV.

It is necessary, then, to calculate the dispersion relation $\epsilon(\boldsymbol{k})$. Following the tight binding model we can describe it as a function of hopping parameters t_i, lattice parameters a and b, and the wavevector $\boldsymbol{k}$:

$$\begin{aligned}\epsilon(\boldsymbol{k}) = &-2t_0(\cos(k_x a) + \cos(k_y b)) - 4t_1\cos(k_x a)\cos(k_y b) - 2t_2(\cos(2k_x a) + \cos(2k_y b)) \\ &- 4t_3(\cos(2k_x a)\cos(k_y b) + \cos(2k_y b)\cos(k_x a)) \\ &- 2t_4\cos(2k_x a)\cos(2k_y b) - E_f\end{aligned} \tag{5.3}$$

E_f is the Fermi energy, simply set to 0 by convention in a normal case. We use the parameters found by Markiewicz, Bansil, and Das [24] fit to overdoped (Pb,Bi)-2201 ($x = 0.38$). Calculations using these parameters yield a Fermi surface depicted in Figure 5-4 [24].

To calculate the self-energy we use a conventional BCS model for a gap with $d_{x^2-y^2}$ symmetry,

$$\Sigma(\boldsymbol{k},\omega) = \frac{|\Delta(\boldsymbol{k})|^2}{\omega + i\Gamma + \epsilon(\boldsymbol{k})} \tag{5.4}$$

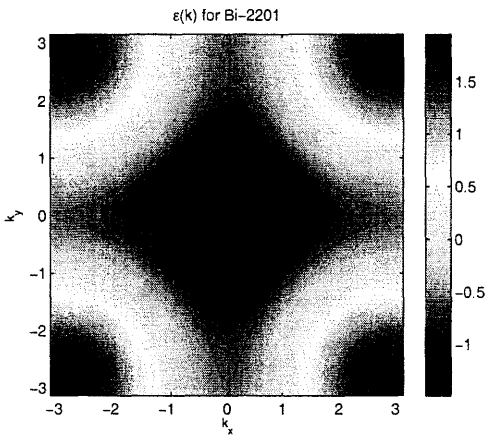

Figure 5-4: Equation (5.3) is used to model the Fermi surface, which exhibits a hole-like structure.

such that the gap is described by

$$\Delta(\boldsymbol{k}) = \Delta_0(\cos(k_x * a) - \cos(ky * a)) \ . \tag{5.5}$$

Δ_0 is adjusted to match the observed spectral width.

5.3 The van Hove scenario

Van Hove, in his seminal 1953 paper [31], derived the effects of saddle points in the Fermi surface on the spectral function. In a two-dimensional crystal, a saddle point will result in a discontinuity in the density of states, while in a three-dimensional crystal a saddle point leads to a discontinuity in the derivative and a sharp peak in the density of states. The Fermi surface for our sample has saddle points at $(0, \pm\pi)$ and $(\pm\pi, 0)$, so the prevalence of sharp peaks we observe is in line with this picture, known as the van Hove scenario [23, 30].

The existence of a "van Hove singularity" (VHS) is known to account for a very diverse set of tunneling spectra, given that the width of the modeled spectrum can be adjusted by the barrier and broadening parameters while the peak height and asymmetry can be adjusted by the band structure parameters [32]. We hypothesize that the spectra we observe in (Pb,Bi)-2201 are manifestations of the van Hove sin-

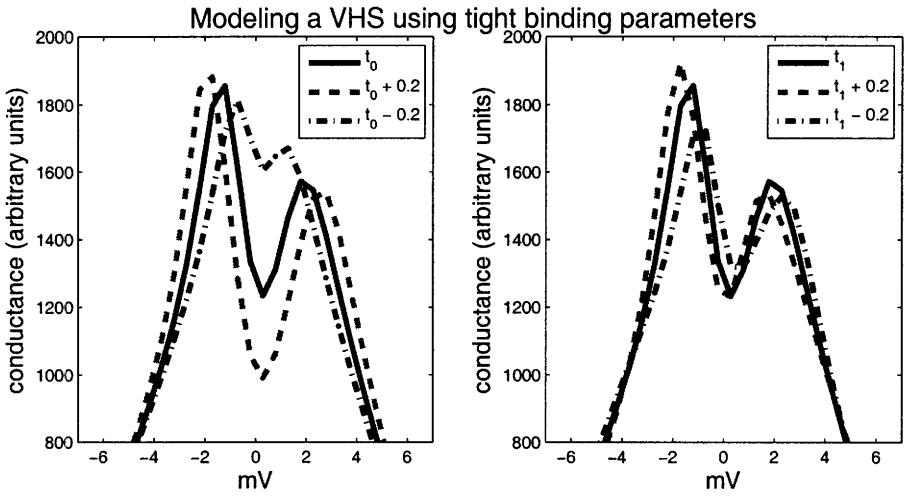

Figure 5-5: Under the VHS model, we can adjust the spectral characteristics by modifying band structure parameters. In these plots the thick blue line represents the calculation done with the parameters given above, while red dashed and black dot-dashed lines show the resulting shifts from parameter changes. The left plot shows the effect of t_0 on peak location and the right plot shows tilting on spectral weight by changing t_1.

gularity and proceed to make those adjustments in order to demonstrate the model's applicability.

5.4 Spectral analysis

Qualitatively, the van Hove scenario appears to account for a good deal of the spectral features we observe in (Pb,Bi)-2201. Although the rare gapped regions are unaccounted for, a comparison of theoretical modeling of the VHS (Fig. 5-5) to our observations (Fig. 5-2) suggests that the spectra we measure can be described in this way. The VHS model includes a lower secondary peak separated by a distance from the tallest peak, as well as the steeper outer slope on the higher peak side. Positive VHS energies result in peak positions below $E_f = 0$ while negative energies push the peak above it.

The VHS model spectra $f_{VHS}(E)$ were fit to recorded dI/dV curves using the formula $\frac{dI(E)}{dV} = a_0 f_{VHS}(a_1 E + a_2) + a_3$. The integration within the theoretical model makes numerically fitting an extremely computationally intensive process, therefore

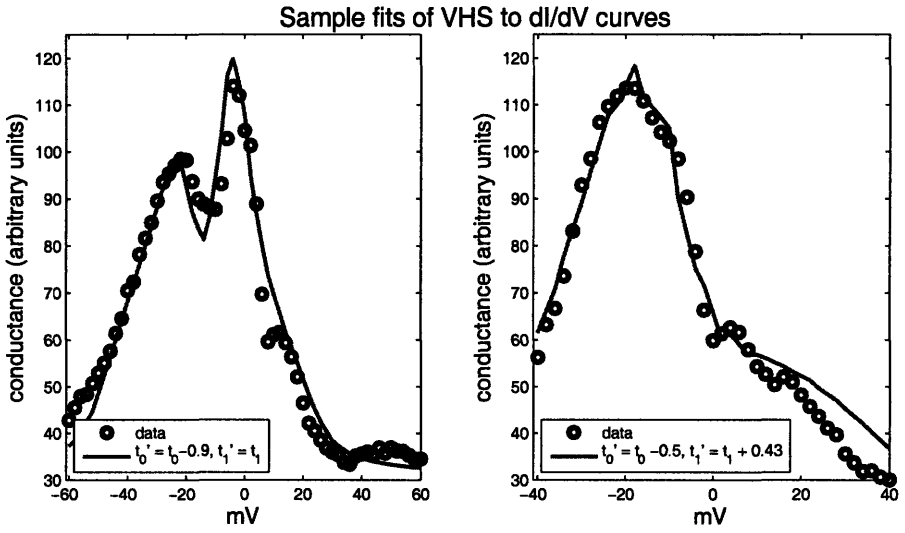

Figure 5-6: Observed tunneling data is fit with the VHS model using the formula $\frac{dI(E)}{dV} = a_0 f_{VHS}(a_1 E + a_2) + a_3$. The left spectrum represents a VHS energy of -0.55 mV while the right spectrum has a VHS energy of 1.17 mV.

the fits shown here were adjusted by hand until a reduced χ^2 value of less than 4.5 was reached. Modifying the first and second hopping parameters t_0 and t_1 was sufficient to model the wide variety of spectra to within this degree of accuracy (see examples in Fig. 5-6). Most of the fitting error occurred near the base of the peak structure. A larger background structure may be affecting the spectrum there while not being large enough to prevent the van Hove singularity from appearing clearly.

Although the a_0 term, the scaling of the model function, is dependent upon the resolution used in numerical integration, it remained at a constant value while at that resolution, which is indicative of a real scaling effect (for example, the ignored $|T_k|^2$ term in (5.1)). The other parameters - a vertical shift in dI/dV, a horizonal shift in ω, and a scaling term applied ω - may have explanations in data acquisition settings, or potentially more interesting physics.

Also interesting to note is the asymmetry consistency: spectra which were mapped to a high peak bias in Figure 5-3, when individually examined, show a smaller peak at a lower bias, which is subsequently accounted for by the VHS model with a high E_{VHS}. Similarly, spectra mapped to low peak bias have a smaller peak at high bias, represented by a low E_{VHS}.

Chapter 6

Conclusions

The high resolution of scanning tunneling microscopy and spectroscopy has proven a useful tool to examine the properties of (Pb,Bi)-2201. Studying the material in the far overdoped regime where T_c <2K has allowed for the characterization of a region of the phase diagram which lies at the junction of the superconducting, pseudogapped, and metallic regions. Here we find differential tunneling spectra that resemble conductance peaks. I have shown that they are well-modeled by a van Hove singularity. The data confirm the uniform random distribution of lead atoms throughout the sample and a lack of relationship between spectral features and Pb location. However, the van Hove energy does appear to change as a function of the structural modulations which are not completely removed by the lead substitution. An adjustment of the tight binding parameters has been shown to account for the changes in spectra which occur when the lattice is strained.

This thesis has helped to build the foundation for a description of spectra using the van Hove scenario. Further characterization and physical interpretation of the phenomenon, such as a large-scale investigation of the fitting parameters, may prove useful in describing the big picture. The VHS approach has been applied in the underdoped and optimally doped regimes of cuprates as well, and factors which are constant throughout these models could indicate generalizable attributes. Future studies may also look into the mechanism behind the residual supermodulations we observed; while they were convenient here because they allowed comparisons of spec-

tra in modulated and unmodulated regions, the interesting question still remains of why a quantity of lead substitution sufficient to smooth the BiO plane in an optimally doped sample would be insufficient in samples in the overdoped regime.

Bibliography

[1] B. M. Andersen, P. Hirschfeld, and J. A. Slezak. Superconducting gap variations induced by structural supermodulation in BSCCO. *arXiv:cond-mat.supr-con*, Apr 2007.

[2] J. Bardeen, L. N. Cooper, and J. R. Schrieffer. Theory of superconductivity. *Phys. Rev.*, 108(5):1175–1204, Dec 1957.

[3] J. Bednorz and K. Müller. Possible high-T_c superconductivity in the Ba-La-Cu-O system. *Z. Phys. B*, 1986.

[4] G. Binnig, H. Rohrer, C. Gerber, and E. Weibel. Surface studies by scanning tunneling microscopy. *Phys. Rev. Lett.*, 49(1):57–61, Jul 1982.

[5] I. Chong, T. Terashima, Y. Bando, M. Takano, Y. Matsuda, T. Nagaoka, and K. ichi Kumagai. Growth of heavily Pb-substituted Bi-2201 single crystals by a floating zone method. *Physica C: Superconductivity*, 290:57–62, Oct. 1997.

[6] A. Damascelli, Z. Hussain, and Z. X. Shen. Angle-resolved photoemission studies of the cuprate superconductors. *Rev. Mod. Phys.*, 75(2):473–541, Apr 2003.

[7] A. Damascelli, D. H. Lu, and Z. X. Shen. From mott insulator to overdoped superconductor: Evolution of the electronic structure of cuprates studied by arpes. *J. Electron. Spectr. Relat. Phenom.*, 165, 2001.

[8] H. Ding, T. Yokoya, J. Campuzano, T. Takahashi, M. Randeria, M. Norman, T. Mochiku, K. Kadowaki, and J. Giapintzakis. Spectroscopic evidence for a

pseudogap in the normal state of underdoped high-t_c superconductors. *Nature*, 382:51–54, July 1996.

[9] D. L. Feng, A. Damascelli, K. M. Shen, N. Motoyama, D. H. Lu, H. Eisaki, K. Shimizu, J.-i. Shimoyama, K. Kishio, N. Kaneko, M. Greven, G. D. Gu, X. J. Zhou, C. Kim, F. Ronning, N. P. Armitage, and Z.-X. Shen. Electronic structure of the trilayer cuprate superconductor $Bi_2Sr_2Ca_2Cu_3O_{10+\delta}$. *Phys. Rev. Lett.*, 88(10):107001, Feb 2002.

[10] V. Ginzburg and L. Landau. On the thoery of superconductivity. *Zh. Eksper. Teoret. Fiz.*, 1950.

[11] B. W. Hoogenboom, C. Berthod, M. Peter, O. Fischer, and A. A. Kordyuk. Modeling scanning tunneling spectra of $Bi_2Sr_2CaCu_2O_{8+\delta}$. *Phys. Rev. B*, 67(22):224502, Jun 2003.

[12] Y. Ikeda, Z. Hiroi, H. Ito, S. Shimomura, M. Takano, and Y. Bando. Bi, Pb-Sr-Cu-O system including a modulation-free superconductor. *Physica C Superconductivity*, 165:189–198, Jan. 1990.

[13] Y. Ikeda, H. Ito, S. Shimomura, Y. Oue, K. Inaba, Z. Hiroi, and M. Takano. Phases and their relations in the Bi-Sr-Cu-O system. *Physica C Superconductivity*, 159:93–104, June 1989.

[14] Y. Ikeda, M. Takano, Z. Hiroi, K. Oda, H. Kitaguchi, J. Takada, Y. Miura, Y. Takeda, O. Yamamoto, and H. Mazaki. The high-T_c phase with a new modulation mode in the Bi,Pb-Sr-Ca-Cu-O system. *Jpn. J. Appl. Phys.*, 27(11):L2067–L2070, 1988.

[15] Z. Iqbal, T. Datta, D. Kirven, A. Lungu, J. C. Barry, F. J. Owens, A. G. Rinzler, D. Yang, and F. Reidinger. Superconductivity above 130 K in the Hg-Pb-Ba-Ca-Cu-O system. *Phys. Rev. B*, 49(17):12322–12325, May 1994.

[16] Y. Ito, A.-M. Vlaicu, T. Mukoyama, S. Sato, S. Yoshikado, C. Julien, I. Chong, Y. Ikeda, M. Takano, and E. Y. Sherman. Detailed structure of a pb-doped $Bi_2Sr_2CuO_6$ superconductor. *Phys. Rev. B*, 58(5):2851–2858, Aug 1998.

[17] S. Kaneko, K. Akiyama, M. Mitsuhashi, Y. Hirabayashi, S. Ohya, K. Seo, H. Funakubo, A. Matsuda, and M. Yoshimoto. Effect of oxygen pressure on structural modulation observed by X-ray reciprocal space mapping in epitaxial bismuth cuprate superconducting film. *Europhys. Lett.*, 71(4):686, 2005.

[18] G. Kinoda, T. Hasegawa, S. Nakao, T. Hanaguri, K. Kitazawa, K. Shimizu, J. Shimoyama, and K. Kishio. Observations of electronic inhomogeneity in heavily pb-doped $Bi_2Sr_2CaCu_2O_y$ single crystals by scanning tunneling microscopy. *Phys. Rev. B*, 67(22):224509, Jun 2003.

[19] M. Kugler, O. Fischer, C. Renner, S. Ono, and Y. Ando. Scanning tunneling spectroscopy of $Bi_2Sr_2CuO_{6+\delta}$: New evidence for the common origin of the pseudogap and superconductivity. *Phys. Rev. Lett.*, 86(21):4911–4914, May 2001.

[20] K. Lang, V. Madhavam, J. Hoffman, E. Hudson, H. Eisaki, S. Uchida, and J. Davis. Imaging the granular structure of high-t_c superconductivity in underdoped $Bi_2Sr_2CaCu_2O_{8+\delta}$. *Nature*, 415:412–416, 2002.

[21] A. Loeser, Z. Shen, D. Dessau, D. Marshall, C. Park, P. Fournier, and A. Kapitulnik. Excitation gap in the normal state of underdoped Bi2Sr2CaCu2o8+δ. *Science*, page 325, July 1996.

[22] G. D. Mahan. *Many-particle Physics*. Plenum Press, New York, 1990.

[23] R. Markiewicz. Van Hove Jahn-Teller effet and high-T_c superconductivity. *J. Phys. Chem. Solids*, 58:1179, 1997.

[24] R. Markiewicz, A. Bansil, and T. Das. Tight-binding parameters for (Pb/La)-Bi2201 at several dopings. *Unpublished*, 2007.

[25] H. Mashima, N. Fukuo, Y. Matsumoto, G. Kinoda, T. Kondo, H. Ikuta, T. Hitosugi, and T. Hasegawa. Electronic inhomogeneity of heavily overdoped $Bi_{2-x}Pb_xSr_2CuO_y$ studied by low-temperature scanning tunneling microscopy/spectroscopy. *Physical Review B (Condensed Matter and Materials Physics)*, 73(6):060502, 2006.

[26] K. McElroy, J. Lee, J. Slezak, D.-H. Lee, H. Eisaki, S. Uchida, and J. Davis. Atomic-scale sources and mechanism of nanoscale electronic disorder in $Bi_2Sr_2CaCu_2O_{8+\delta}$. *Science*, 309(5737):1048–1052, 2005.

[27] T. Motohashi, Y. Nakayama, T. Fujita, K. Kitazawa, J. Shimoyama, and K. Kishio. Systematic decrease of resistivity anisotropy in $Bi_2Sr_2CaCu_2O_y$ by Pb doping. *Phys. Rev. B*, 59(21):14080–14086, Jun 1999.

[28] T. S. Nunner, B. M. Andersen, A. Melikyan, and P. J. Hirschfeld. Dopant-modulated pair interaction in cuprate superconductors. *Physical Review Letters*, 95(17):177003, 2005.

[29] H. Onnes. The resistance of pure mercury at helium temperatures. *Comm. Phys. Lab. Univ. Leiden*, 1911.

[30] J. Storey, J. Tallon, and G. Williams. Thermodynamic properties of $Bi_2Sr_2CaCu_2O_8$ calculated from the electronic dispersion. *arXiv:cond-mat.supr-con*, Apr 2007.

[31] L. Van Hove. The occurrence of singularities in the elastic frequency distribution of a crystal. *Phys. Rev.*, 89(6):1189–1193, Mar 1953.

[32] J. Y. T. Wei, C. C. Tsuei, P. J. M. van Bentum, Q. Xiong, C. W. Chu, and M. K. Wu. Quasiparticle tunneling spectra of the high-T_c mercury cuprates: Implications of the d-wave two-dimensional van Hove scenario. *Phys. Rev. B*, 57(6):3650–3662, Feb 1998.

[33] H. W. Zandbergen, W. A. Groen, F. C. Mijlhoff, G. van Tendeloo, and S. Amelinckx. Models for the modulation in $A_2B_2Ca_nCu_{1+n}O_{6+2n}$, A, B=Bi,

Sr or Tl, Ba and n=0, 1, 2. *Physica C Superconductivity*, 156:325–354, Oct. 1988.